The Measurement of Neutrino Properties with Atmospheric Neutrinos

Takaaki Kajita

Institute for Cosmic Ray Research and the Kavli Institute for the Physics and Mathematics of the Universe, University of Tokyo, Kashiwa, Chiba 277-8582, Japan; email: kajita@icrr.u-tokyo.ac.jp

Annu. Rev. Nucl. Part. Sci. 2014. 64:343–62

First published online as a Review in Advance on July 21, 2014

The *Annual Review of Nuclear and Particle Science* is online at nucl.annualreviews.org

This article's doi:
10.1146/annurev-nucl-102313-025402

Keywords

neutrinos, atmospheric neutrinos, neutrino oscillation, cosmic rays

Abstract

Atmospheric neutrinos are produced by cosmic-ray interactions in the atmosphere. Atmospheric neutrino experiments typically observe zenith-angle and energy dependences of ν_μ and ν_e events. Through these experiments, neutrino oscillation was discovered. Since then, various studies have been performed to further our understanding of neutrino properties. This article discusses experimental studies of neutrino oscillations with atmospheric neutrinos.

Contents

1. INTRODUCTION

Atmospheric neutrinos are produced by cosmic-ray interactions in the atmosphere. High-energy cosmic-ray interactions with air nuclei produce secondary particles. The most abundantly produced particles are pions, which decay to other particles:

$$\begin{aligned} \pi^+ &\to \mu^+ + \nu_\mu, \\ \mu^+ &\to e^+ + \bar{\nu}_\mu + \nu_e, \end{aligned}$$

$$\begin{aligned} \pi^- &\to \mu^- + \bar{\nu}_\mu, \\ \mu^- &\to e^- + \nu_\mu + \bar{\nu}_e. \end{aligned} \qquad 1.$$

Atmospheric neutrino experiments study these neutrinos produced in the Earth's atmosphere.

The small but finite neutrino masses can be understood naturally by the seesaw mechanism (1–3) through the introduction of superheavy neutral particles. Continuing experiments are searching for nonzero neutrino masses. One way to search for these masses is to study neutrino oscillations (4, 5). Neutrino oscillation is a phenomenon in which a neutrino produced in a definite type (flavor) is later observed in a different flavor after traveling some distance.

If neutrinos have finite masses, then each flavor eigenstate (for example, ν_μ) can be expressed by a combination of mass eigenstates (ν_1, ν_2, and ν_3). The relation between the mass eigenstates (ν_1, ν_2, and ν_3) and the flavor eigenstates (ν_e, ν_μ, and ν_τ) can be expressed by

$$\begin{pmatrix} \nu_e \\ \nu_\mu \\ \nu_\tau \end{pmatrix} = U \cdot \begin{pmatrix} \nu_1 \\ \nu_2 \\ \nu_3 \end{pmatrix}, \qquad 2.$$

where U is the mixing matrix. U is expressed by

$$U = \begin{pmatrix} c_{12}c_{13} & s_{12}c_{13} & s_{13}e^{-i\delta} \\ -s_{12}c_{23} - c_{12}s_{23}s_{13}e^{i\delta} & c_{12}c_{23} - s_{12}s_{23}s_{13}e^{i\delta} & s_{23}c_{13} \\ s_{12}s_{23} - c_{12}c_{23}s_{13}e^{i\delta} & -c_{12}s_{23} - s_{12}c_{23}s_{13}e^{i\delta} & c_{23}c_{13} \end{pmatrix}, \qquad 3.$$

where c_{ij} and s_{ij} represent $\cos\theta_{ij}$ and $\sin\theta_{ij}$, respectively.

For simplicity, let us assume that neutrino oscillation is purely between a ν_μ and a ν_τ. The probability that a ν_μ survives as a ν_μ after traveling some distance L is expressed as

$$P(\nu_\mu \rightarrow \nu_\mu) = 1 - \sin^2 2\theta_{23} \cdot \sin^2 \left(\frac{1.27 \Delta m^2_{23}(\mathrm{eV}^2) L(\mathrm{km})}{E_\nu(\mathrm{GeV})} \right), \quad 4.$$

where E_ν is the neutrino energy and $\Delta m_{23}{}^2$ is the mass-squared difference between the neutrino mass eigenstates ($|m_2^2 - m_3^2|$).

Equation 4 indicates that, if one wants to observe smaller neutrino masses, one has to observe neutrinos that travel longer distances, such as atmospheric neutrinos. The flight length of these neutrinos ranges up to 12,700 km, the diameter of the Earth. Assuming the typical atmospheric neutrino energy of 1 GeV, one can estimate that atmospheric neutrinos are sensitive to neutrino oscillations if $\Delta m_{23}{}^2$ is larger than $\sim 10^{-4}$ eV^2. Indeed, the small neutrino mass was determined through the study of these neutrinos.

The above two-flavor oscillation formula (Equation 4) has to be generalized to three-flavor oscillations. In the three-flavor oscillation framework, neutrino oscillations are parameterized by three mass-squared differences ($\Delta m_{12}{}^2$, $\Delta m_{23}{}^2$, and $\Delta m_{13}{}^2$; among the three, only two are independent), together with the three mixing angles and one *CP* phase listed in the mixing matrix. As discussed in Sections 3 and 4, so far θ_{23} and $\Delta m_{23}{}^2$ ($\sim \Delta m_{13}{}^2$) have been the most relevant to atmospheric neutrino experiments. θ_{12} and $\Delta m_{12}{}^2$ have been measured by solar and long-baseline reactor neutrino experiments. Most recently, θ_{13} was measured by accelerator-based long-baseline and reactor neutrino oscillation experiments.

Due to the hierarchies $\Delta m_{12}{}^2 \ll \Delta m_{23}{}^2, \Delta m_{13}{}^2$ and $\theta_{13} \ll \theta_{12}, \theta_{23}$, it is approximately correct to assume two-flavor oscillations for analyses of many existing neutrino oscillation data. Therefore, in the first few sections of this review, we discuss the atmospheric neutrino data in terms of $\nu_\mu \rightarrow \nu_\tau$ two-flavor neutrino oscillations. In the remaining sections, we extend our discussion to full three-flavor oscillations.

2. ATMOSPHERIC NEUTRINOS AND THEIR FLUX

In the GeV/nucleon energy region, cosmic-ray particles consist mostly of protons, followed by $\sim$5% helium nuclei and a still-smaller fraction of heavier nuclei. These particles interact with the nuclei in the atmosphere high above the Earth. In these high-energy cosmic-ray interactions with nuclei, many pions (and, less abundantly, kaons) are produced. These pions decay to other particles (Equation 1). Similar decay processes occur for kaons and other particles. In this manner, neutrinos are produced. The production of atmospheric neutrinos is depicted in **Figure 1**. The primary cosmic-ray flux decreases rapidly with energy, approximately $E^{-2.7}$ in the GeV–TeV energy region. Therefore, the calculated neutrino flux rapidly decreases with increasing energy.

Equation 1 indicates that two (ν_μ plus $\bar{\nu}_\mu$) and one (ν_e or $\bar{\nu}_e$) are produced for one charged-pion decay. Because the energies of these neutrinos are almost equal, the ratio of the $(\nu_\mu + \bar{\nu}_\mu)$ and $(\nu_e + \bar{\nu}_e)$ fluxes should be approximately two. Indeed, detailed calculations of the neutrino flux have determined that this ratio is very close to two. The accuracy of the calculated ratio is estimated to be better than a few percent in the GeV energy range. This flux ratio is a good indicator of neutrino oscillations, given that it should deviate from the predicted ratio if neutrinos oscillate. As described below, the first serious indication of neutrino oscillation was observed through the study of this ratio.

Figure 2 shows the calculated $(\nu_\mu + \bar{\nu}_\mu)/(\nu_e + \bar{\nu}_e)$, $\nu_\mu/\bar{\nu}_\mu$, and $\nu_e/\bar{\nu}_e$ flux ratios as a function of the neutrino energy (6). Clearly, the $(\nu_\mu + \bar{\nu}_\mu)/(\nu_e + \bar{\nu}_e)$ ratio is approximately two below $E_\nu \cong 1$ GeV, where most of the muons produced by the pion decays are expected to decay before

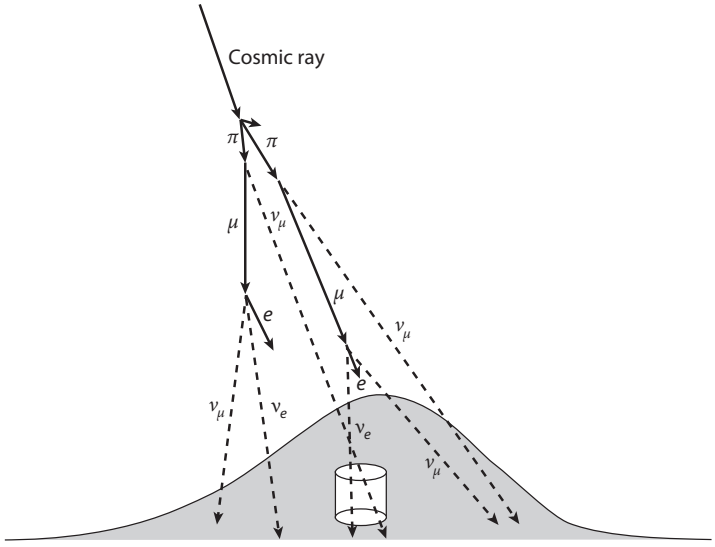

Figure 1

Production of neutrinos by cosmic-ray interactions with air nuclei in the atmosphere. Neutrino production in the atmosphere typically occurs at an altitude of 15 km.

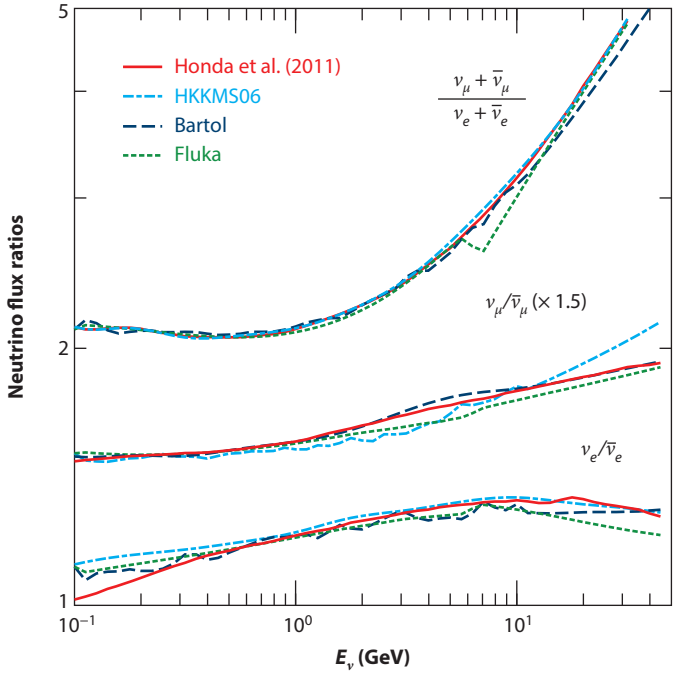

Figure 2

Calculated $(\nu_\mu + \bar{\nu}_\mu)/(\nu_e + \bar{\nu}_e)$, $\nu_\mu/\bar{\nu}_\mu$, and $\nu_e/\bar{\nu}_e$ flux ratios of atmospheric neutrinos as a function of neutrino energy by three independent groups (6–9).

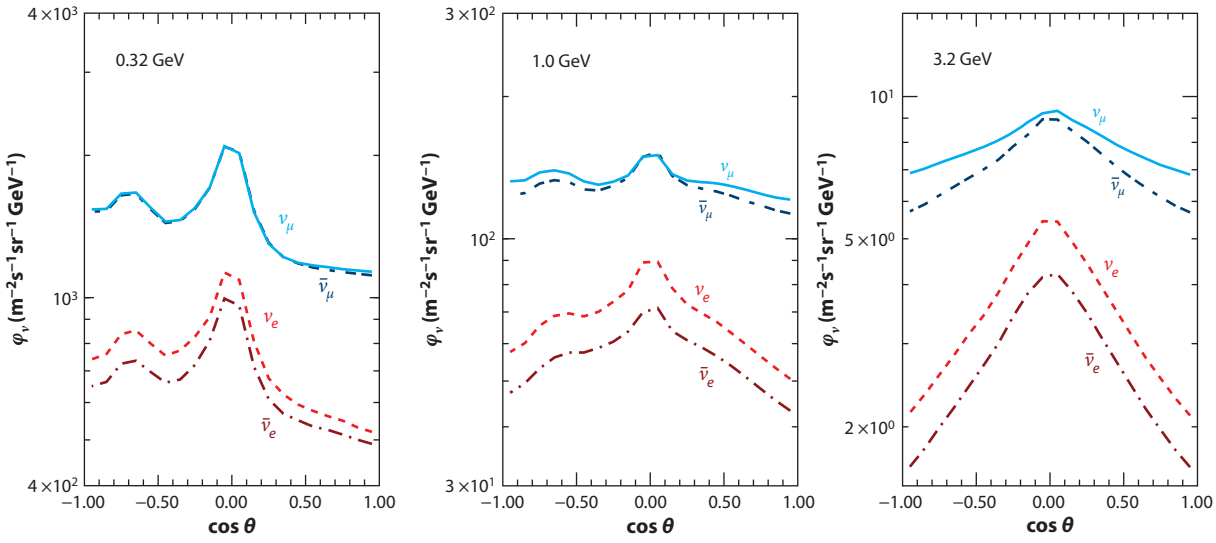

Figure 3

Calculated zenith-angle dependence of the atmospheric neutrino flux for several neutrino energies at Kamioka, Japan (6).

reaching the ground. Above this energy range, the ratio increases due to the increasing probability of muons reaching the ground before their decay. Also, this ratio has been accurately calculated, given that the results from three independent calculations (6–9) agree well. Note that the $\nu_\mu/\bar{\nu}_\mu$ and $\nu_e/\bar{\nu}_e$ ratios have also been accurately calculated.

Another important feature of the atmospheric neutrino flux is its up–down symmetry. A neutrino thus produced enters the Earth at a point pos_{in} with a zenith angle θ_{in} and should exit at a point pos_{out} with a zenith angle $\pi - \theta_{\text{in}}$. Because a cosmic ray enters the atmosphere at approximately the same rate at any position, there must be a neutrino that enters and exits at the same points with the same zenith angles. These two processes occur at equal rates insofar as the primary cosmic-ray fluxes in both positions are equal. Thus, the flux should be up–down symmetric (10). As discussed in Section 3 below, a comparison between the up–down asymmetry of the experimental data and the prediction provided compelling evidence for neutrino oscillations and has been used to measure the neutrino mixing angle.

Figure 3 shows the calculated zenith-angle dependence of the atmospheric neutrino flux for several neutrino energies at Kamioka, Japan (6). In fact, above a few GeV, the flux is up–down symmetric. Below this energy, the flux is not exactly up–down symmetric because of the geomagnetic field: Low-energy cosmic-ray particles are bent significantly by the geomagnetic field, and only cosmic-ray particles above a certain rigidity (momentum/charge, GeV/$c\ z^{-1}$), which depends on latitude and longitude and on the direction of the cosmic-ray particles, can enter the atmosphere. The cutoff rigidities for vertically entering cosmic rays near the geomagnetic poles and equator are <1 GeV/$c\ z^{-1}$ and $\sim$15 GeV/$c\ z^{-1}$, respectively. Thus, the flux of low-energy, downward-going neutrinos depends on the local geomagnetic field above the detector, whereas the flux of low-energy, upward-going neutrinos is more or less averaged out by integrating over the whole Earth. Because cosmic-ray particles with primary energy E contribute to the neutrino flux in the energy range of 0.1 E, the geomagnetic-field effect can produce sizable up–down asymmetry only in the sub-GeV energy range.

Finally, note that experimental studies of atmospheric neutrinos motivated improvements in the flux calculation. In the 1980s and 1990s, the uncertainty in the absolute neutrino flux calculation was at least 20% in the GeV energy range. Because atmospheric neutrino experiments required a better understanding of the flux, flux calculations (as well as measurements of the primary cosmic-ray and secondary cosmic-ray muon fluxes) have been improved. As of 2013, the uncertainty in the absolute flux normalization is estimated to be 7–8% between 1- and 10-GeV neutrino energies (6, 7).

3. EARLY MEASUREMENTS OF ATMOSPHERIC NEUTRINO PROPERTIES AND THE DISCOVERY OF NEUTRINO OSCILLATIONS

Observations of atmospheric neutrinos began in the mid 1960s. Two experiments performed in extremely deep mines in India (11) and South Africa (12) successfully observed muons produced by atmospheric ν_μ interactions.

In the early 1980s, several proton decay experiments began. The masses of the detectors ranged from ∼100 to 3,000 tons to enable observation of proton decays that had been predicted by early Grand Unified Theories (13, 14). These experiments did not observe any convincing signal of proton decays. However, they did observe hundreds of atmospheric neutrino interactions. Proton decay and atmospheric neutrino events can be separated only by studying the properties of the secondary particles. Therefore, these experiments studied the details of the neutrino events.

A piece of information that is important for the study of neutrino oscillations is the type of particles produced. An electron produced in a detector by a ν_e interaction propagates in the medium, producing an electromagnetic shower, whereas a muon produced by a ν_μ interaction propagates in the medium, losing the energy slowly without producing an electromagnetic shower. Kamiokande and Irvine–Michigan–Brookhaven (IMB) were water Cherenkov detectors; photomultiplier tubes installed on the detectors' walls enabled imaging of Cherenkov radiation. The image from an electron is the summation of the ring images of many electrons and positrons in the electromagnetic shower and is characterized by a fuzzy ring pattern, whereas the image from a muon is produced only by the muon and has a clearer ring pattern. Therefore, it is possible to distinguish Cherenkov rings from electrons and from muons; these rings are referred to as e-like and μ-like, respectively, for the remainder of this review.

In 1988, Kamiokande reported the numbers of observed μ-like and e-like events (15). The observed number of e-like events in the data (93) agreed with the corresponding prediction (88.5) within statistical error. However, the observed number of μ-like events (85) was much smaller than the prediction (144). Because the probability of misidentification of the particle types was estimated to be 2%, it was not possible to attribute this result to a bias in particle identification. Also, as discussed above, the ν_μ/ν_e ratio of the flux had been accurately predicted.

Neutrino oscillations between ν_μ and ν_τ or between ν_e and ν_μ could change the ν_μ/ν_e flux ratio from approximately two to one and, hence, could explain the results. However, this change requires a large mixing angle, which was not commonly believed to be the case—the corresponding mixing angles between the quarks were known to be small.

The 1988 Kamiokande result (15) was the beginning of serious interest in atmospheric neutrinos. Consistent results were reported from the IMB water Cherenkov experiment in 1991 (16); from the Soudan-2 experiment, which used an iron calorimeter detector, in 1997 (17); and from an updated analysis of the Kamiokande data in 1992 (18).

Another important development in our understanding of the atmospheric neutrino problem occurred in the mid 1990s. If the observed ν_μ deficit is due to neutrino oscillations, then the deficit

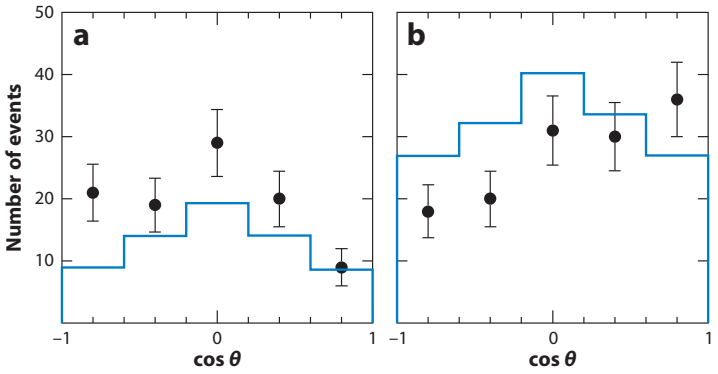

Figure 4

Zenith-angle distributions for multi-GeV (*a*) fully contained *e*-like events and (*b*) fully contained plus partially contained μ-like events observed in Kamiokande (19), where multi-GeV means larger than 1.33 GeV of visible energy. Each histogram shows the predicted distributions without oscillations. The absolute normalization has an uncertainty of at least 20%.

should depend on the neutrino flight length and, therefore, on the zenith angle. However, in the energy range below ~1 GeV, the angular correlation between the neutrino and muon directions is rather poor. The zenith-angle dependence in the neutrino direction is largely washed out in the muon zenith-angle distribution in this energy range. The angular correlation substantially improves with increasing neutrino energy, and the muon zenith-angle distribution should represent the neutrino zenith-angle distribution fairly well for multi-GeV neutrino events.

Zenith-angle distributions for multi-GeV fully contained events and partially contained events were studied in Kamiokande (19). For detectors near the surface of the Earth, the neutrino flight distance and, thus, the neutrino oscillation probability are functions of the zenith angle of the neutrino direction. Vertically downward-going neutrinos travel ~15 km, whereas vertically upward-going neutrinos travel ~12,700 km before interacting in the detector. **Figure 4** shows the zenith-angle distribution for multi-GeV neutrino events observed in Kamiokande. The up–down ratios for multi-GeV μ-like and *e*-like events were $0.58^{+0.13}_{-0.11}$ and $1.38^{+0.39}_{-0.30}$, respectively. The statistical significance of the observed up–down asymmetry for the μ-like events was 2.8σ. However, due to the relatively poor event statistics, the data were not conclusive. Experimental data with much higher statistics were needed.

The Super-Kamiokande detector (**Figure 5**) (20) is a large, cylindrical water Cherenkov detector. It measures 41.4 m in height and 39.3 m in diameter, and its total mass is 50,000 tons. The detector consists of two parts: the inner detector, which studies the details of neutrino interactions, and the outer detector, which identifies the incoming and outgoing charged particles. The fiducial mass is the central 22,500 tons, which is ~20 times larger than that of Kamiokande.

Due to its larger fiducial mass, Super-Kamiokande can accumulate neutrino events ~20 times faster than Kamiokande can. Furthermore, the images of the Cherenkov rings observed by the 11,200 photomultiplier tubes in Super-Kamiokande's inner detector make it possible to study the details of events. **Figure 6** shows the candidate charged-current ν_e and ν_μ interactions with visible single Cherenkov rings observed in Super-Kamiokande. These observations are particularly useful for detailed studies of neutrino oscillations.

The Super-Kamiokande experiment began in April 1996. The analysis methods for the atmospheric neutrino interactions are well known from previous studies of atmospheric neutrinos. By the spring of 1998, Super-Kamiokande had analyzed 535 days of data or, equivalently,

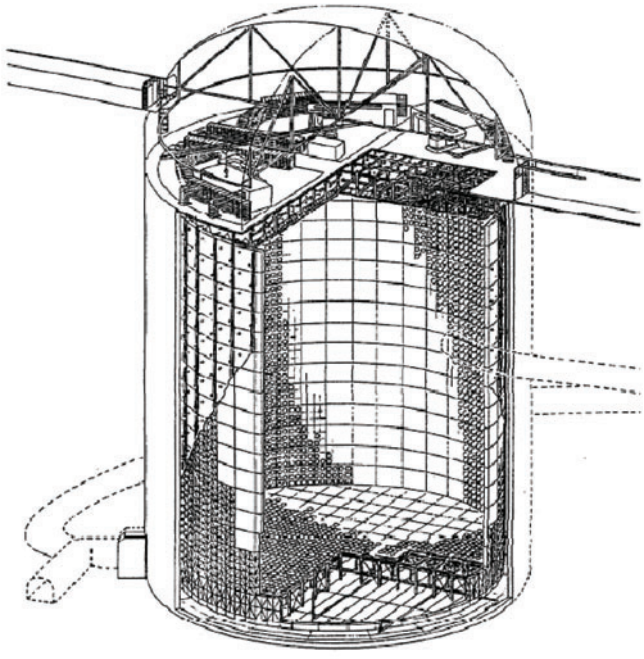

Figure 5

The Super-Kamiokande detector. The inner detector uses ~11,200 photomultiplier tubes. The outer detector is equipped with ~1,900 20-cm-diameter photomultiplier tubes.

33 kiloton-years of detector exposure. The total number of atmospheric neutrino events was ~5,400, which is approximately four times more statistics than those from Kamiokande.

The Super-Kamiokande Collaboration (21, 22) announced evidence for atmospheric neutrino oscillations in 1998. This evidence was obtained from several measurements; the strongest evidence for oscillation came from zenith-angle distributions (**Figure 7**). Clearly, a deficit of upward-going μ-like events had been observed. The statistical significance was more than 6σ, implying that the deficit was not due to a statistical fluctuation. However, the zenith-angle distribution for e-like events did not show any significant up–down asymmetry, suggesting that ν_es do not oscillate as long as the flight length is less than the diameter of the Earth. These data led to the conclusion that ν_μs oscillate to other types of neutrinos, most likely to ν_τs. In addition, the ν_μ/ν_e flux ratio was measured with greater precision for both the sub- and multi-GeV energy ranges, showing significantly smaller ratios than the predictions for both energy ranges. Furthermore, the stopping/through-going flux ratio for upward-going muons and the zenith-angle distribution for upward through-going muons, produced by high-energy atmospheric neutrino interactions in the bedrock below the Super-Kamiokande detector, also required neutrino oscillations to explain the data.

Two other experiments observed atmospheric neutrinos in the late 1990s. One was Soudan-2, which has been taking data since 1989. The data statistics were substantially improved compared with those in earlier publications. Soudan-2 determined the directions of the particles by several

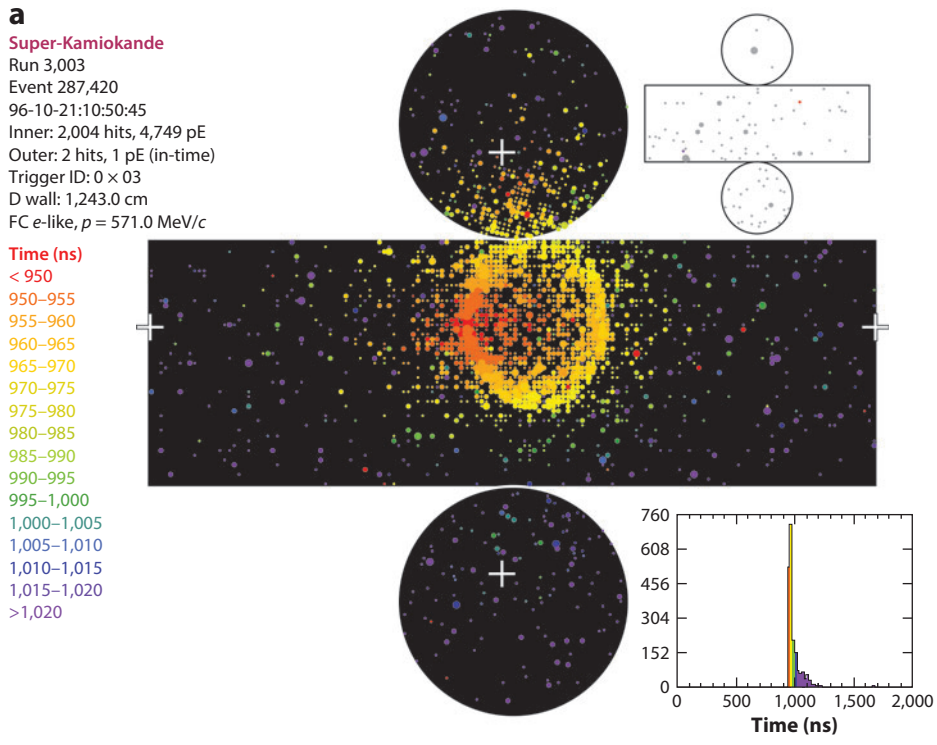

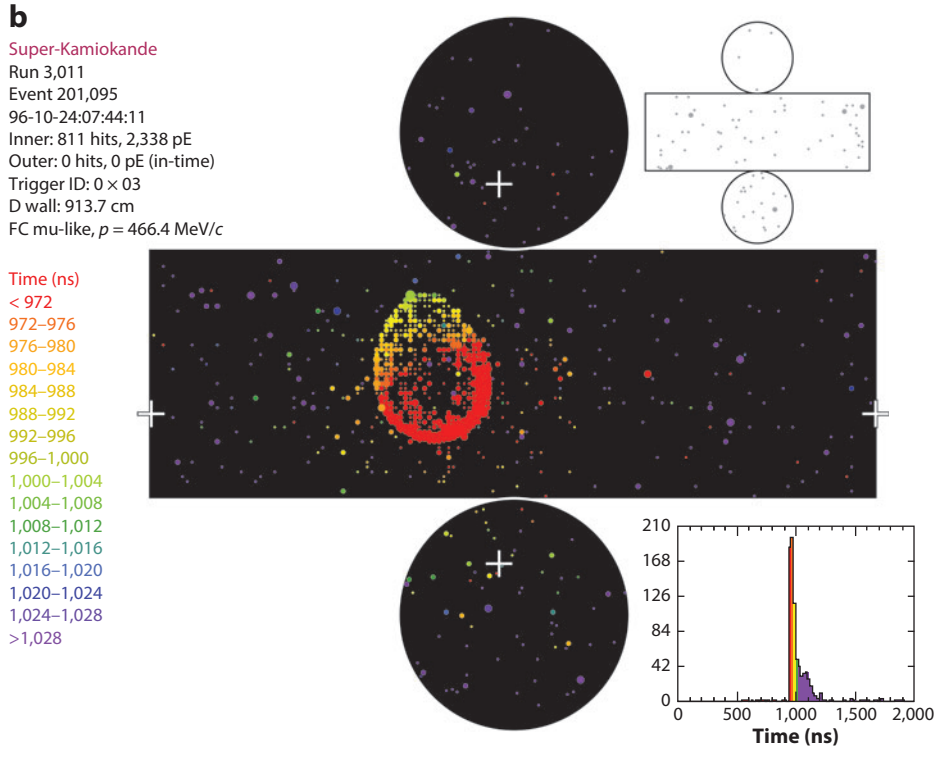

Figure 6

Candidates for charged-current (*a*) ν_e and (*b*) ν_μ interactions with visible single Cherenkov rings observed in Super-Kamiokande. The cylindrical detector is opened flat. The colors indicate the timing of photon detection, and the circle size indicates the pulse height for each photomultiplier tube.

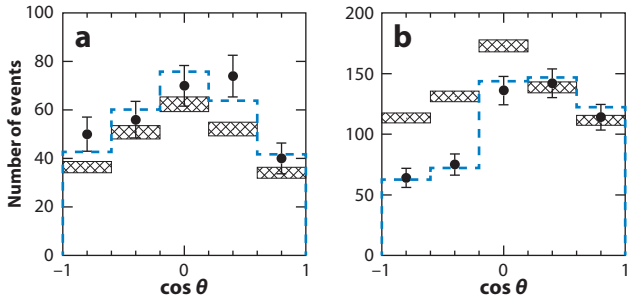

Figure 7

Zenith-angle (θ) distributions for multi-GeV atmospheric neutrino events reported at the Neutrino'98 conference (22) based on 535 days of exposure of the Super-Kamiokande detector. (*a*) The distribution for *e*-like events. (*b*) The distribution for μ-like events. $\cos\theta = 1$ and -1 represent events whose direction is vertically downward going and upward going, respectively.

methods and confirmed the ν_μ deficit as a function of the zenith angle (23). Another experiment was MACRO, a large underground detector that measured upward-going muons as well as partially contained neutrino events. The size of that detector was 12 m $\times$ 77 m $\times$ 10 m (height). This experiment also observed the zenith-angle-dependent deficit of upward-going muons (24) and partially contained ν_μ events (25). The results from these experiments were in good agreement with those from Super-Kamiokande; therefore, the evidence for neutrino oscillation was quickly accepted. Since then, atmospheric neutrino experiments have continued to contribute substantially to our understanding of neutrino properties.

4. RECENT DEVELOPMENTS: FURTHER STUDIES OF NEUTRINO OSCILLATIONS

The 1998 data from Super-Kamiokande showed that ~50% of ν_μs disappear after traveling long distances, and were interpreted to reveal neutrino oscillations. However, several unanswered questions remained: What are the precise values of the neutrino mass-squared difference ($\Delta m_{23}{}^2$) and the neutrino mixing angle (θ_{23})? Does the ν_μ disappearance probability really oscillate as predicted by the theory of neutrino oscillation? Do ν_μs oscillate to ν_τs, and if so, is it possible to confirm $\nu_\mu \rightarrow \nu_\tau$ oscillations by detecting ν_τ interactions? As of 2013, these questions have been addressed. Finally, note that because there exist three neutrino flavors, we should understand the mixing angles and Δm^2s for three types of neutrinos.

4.1. Measurements of Oscillations and Oscillation Parameters

Five experiments have studied atmospheric neutrinos: Super-Kamiokande, MINOS, SNO, ANTARES and IceCube. SNO, a well-known solar neutrino detector, also measured through-going muons (26). Given that the SNO detector was located 2 km underground, the near-horizontal, downward-going muons were neutrino induced. With the currently known $\Delta m_{23}{}^2$ value, one can easily estimate that the effect of neutrino oscillation is negligibly small for neutrinos that generate these near-horizontal, downward-going muons. Therefore, these muon data can be used to calibrate the atmospheric neutrino flux calculation. The measured near-horizontal downward-going muon flux (26) was 1.22 $\pm$ 0.09 times higher than the flux calculated in Reference 8. This result suggests that the absolute flux normalization in the 100-GeV energy range should be improved by future flux calculations.

MINOS is a long-baseline neutrino oscillation experiment. However, because it is located 2,070 meters water equivalent (m.w.e.) underground and has a mass of 5.4 kilotons, it can also detect atmospheric neutrinos. It is the first magnetized tracking detector for atmospheric neutrinos. MINOS can obtain information about track direction, charge, and momentum. The results from MINOS on the study of separated atmospheric ν_μ and $\bar{\nu}_\mu$ events have been reported (27, 28). The data, based on 37.9 kiloton-years of exposure (28), were consistent with the standard $\nu_\mu \rightarrow \nu_\tau$ oscillations, showing no evidence of a difference in oscillation parameters between neutrinos and antineutrinos.

ANTARES and IceCube are neutrino telescopes whose main purpose is to study very high energy astrophysical neutrinos. The main backgrounds in the search for these astrophysical neutrinos are high-energy atmospheric neutrinos. The atmospheric ν_μ energy spectrum has been measured from 100 GeV to 400 TeV (29) and from 100 GeV to 200 TeV (30). In these energy ranges, the energy loss of a muon is approximately proportional to $\log(E_\mu)$. In this way, the muon and parent neutrino energy spectra can be estimated. The measured spectrum is consistent with (or slightly higher than) the predictions and within the errors. In addition, the flux of atmospheric ν_es has been measured in the energy range from 80 GeV to 6 TeV (31). The data were consistent with the calculated flux.

ANTARES reconstructed the muon energy down to 20 GeV and observed the muon deficit in that energy region (32). Recently, IceCube added eight infill strings, named DeepCore, to the existing IceCube array, enabling the observation of lower-energy (below 100 GeV) neutrinos. DeepCore observed the deficit of ν_μ interactions due to neutrino oscillations. The estimated oscillation parameters from ANTARES and IceCube/DeepCore were consistent with the other measurements (32, 33).

These experiments have contributed to studies of atmospheric neutrinos in various ways. However, as far as neutrino oscillation studies are concerned, the statistics of the atmospheric neutrino events in the relevant energy region are dominated by the data from Super-Kamiokande. Therefore, for the remainder of this review we discuss primarily the atmospheric neutrino results from Super-Kamiokande.

The total number of atmospheric neutrino events observed in Super-Kamiokande between 1996 and 2012 (3,903 days or 240 kiloton-years of exposure) is ~40,000—a factor of seven more events than the data analyzed in 1998. **Figure 8** shows some zenith-angle distributions. Clearly, the event statistics are improved significantly compared with the 1998 data (**Figure 7**).

The Super-Kamiokande Collaboration performed a neutrino oscillation analysis by using these events. The analysis carefully studied and accounted for systematic errors, as they can significantly affect the results. There were more than 100 systematic error terms in this analysis. Some of them are related to the flux, the neutrino interactions, and the detector (see Reference 34 for a slightly earlier version of the systematic error list). Because solar neutrino (35, 36) and KamLAND (37) experiments have measured Δm_{12}^2 and $\sin^2\theta_{12}$, and because reactor experiments [Double Chooz (38), RENO (39), and Daya Bay (40)] and long-baseline neutrino oscillation experiments [T2K (41) and MINOS (42)] have measured $\sin^2 2\theta_{13}$ accurately, Δm_{23}^2 and $\sin^2 2\theta_{23}$ have been estimated using the other oscillation parameters as inputs. The *CP* phase (δ_{CP}) has been treated as a free parameter. **Figure 9** shows the allowed regions of neutrino oscillation parameters (Δm_{23}^2 and $\sin^2 2\theta_{23}$) from the Super-Kamiokande atmospheric neutrino analysis (43), as well as those from accelerator-based long-baseline neutrino oscillation experiments (44, 45). Δm_{23}^2 and $\sin^2 2\theta_{23}$ were measured accurately. In particular, $\sin^2 2\theta_{23}$ was constrained to be >0.93 at 90% CL. The mixing angle is consistent with the maximum mixing ($\sin^2 2\theta_{23} = 1.0$). These parameters were much more accurately measured in this analysis than in 1998 (21).

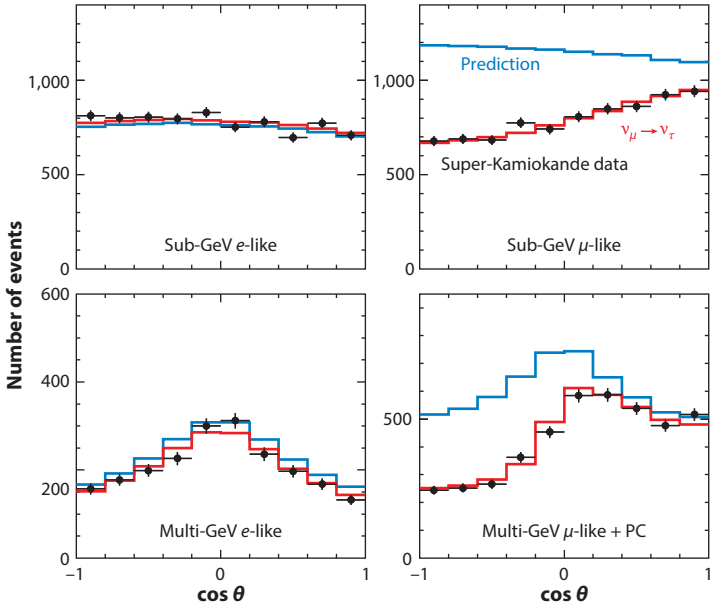

Figure 8

Zenith-angle (θ) distributions observed in Super-Kamiokande during 3,903 days of detector exposure. The blue and red histograms show the nonoscillated and best-fit oscillated Monte Carlo distributions, respectively. Abbreviation: PC, partially contained events.

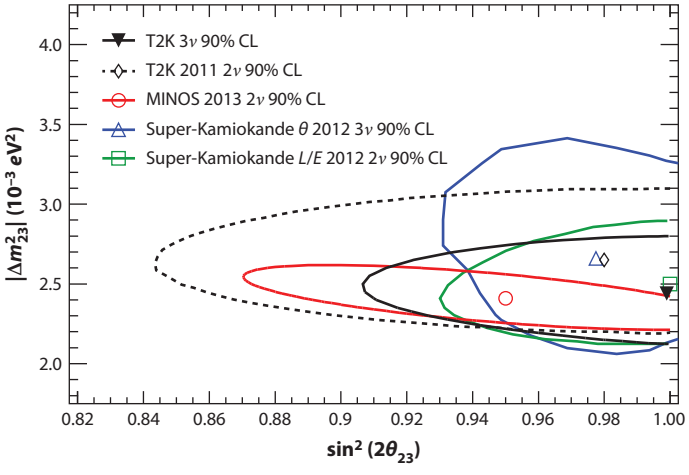

Figure 9

Allowed regions of neutrino oscillation parameters ($\Delta m_{23}{}^2$ and $\sin^2 2\theta_{23}$) at 90% CL from various experiments. The blue and green lines represent the allowed regions based on the zenith-angle (three-flavor) and *L/E* (two-flavor) analyses, respectively, in Super-Kamiokande (preliminary data). Also shown are results from the T2K (44) and MINOS (45) long-baseline experiments. Modified from Reference 44.

We note that the mixing angles differ significantly between quarks and neutrinos. The value $\sin^2 2\theta_{23} > 0.93$ implies that the neutrino mixing angle θ_{23} should be between 37° and 53°, whereas the corresponding mixing angle between quarks is ~2.4°. This difference was not expected before the discovery of neutrino oscillations, and it may help us understand the profound relation between quarks and leptons.

4.2. Observing Oscillations

According to the two-flavor neutrino oscillation formula (Equation 4), the neutrino survival probability should obey the sinusoidal function. The ν_μ survival probability should be a minimum at a certain L/E_ν value, come back to unity after the neutrinos have traveled twice the distance, and then continue oscillating. **Figure 8** depicts atmospheric neutrino events with various L/E_ν in a zenith-angle bin; only an averaged survival probability is observed.

The Super-Kamiokande Collaboration performed a special analysis that used only high-resolution events in L/E_ν. In this analysis, Super-Kamiokande did not use neutrino events whose direction is near the horizon, given that the neutrino flight length, L, changes very significantly for a small variation in the estimated neutrino arrival direction. Also, Super-Kamiokande did not use low-energy neutrino events because the scattering angles in low-energy neutrino interactions are large and, therefore, the uncertainty in the estimated neutrino flight length would be very large. The exclusive use of high L/E_ν resolution events showed that the ν_μ survival probability dips at a position corresponding to the first minimum survival probability (46). **Figure 10** shows the updated L/E_ν plot from Super-Kamiokande (43). When they were published in 2004 (46), these data were the first evidence that the ν_μ survival probability obeys the sinusoidal function, as predicted by neutrino oscillations. The histogram in **Figure 10** shows the expected probability of ν_μ survival from neutrino oscillations, taking the detector resolutions into account. **Figure 9** shows the allowed region of the neutrino oscillation parameters from the two-flavor L/E analysis, together with the other results. This result is consistent with the others.

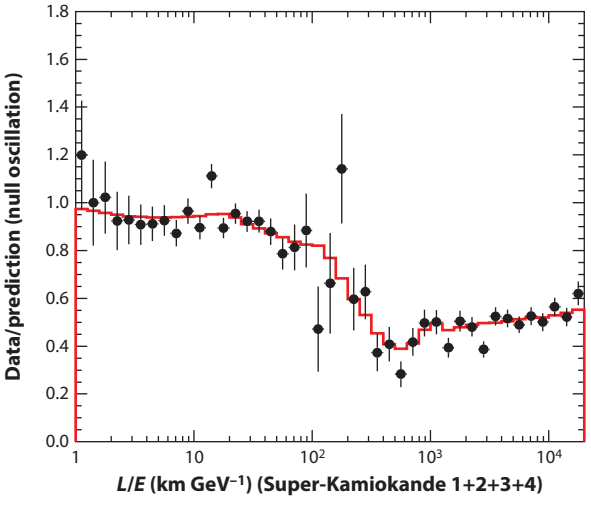

Figure 10

Data over nonoscillated Monte Carlo for μ-like events, plotted as a function of L/E_ν. The red histogram shows the Monte Carlo prediction for $\nu_\mu \rightarrow \nu_\tau$ oscillations. The dip observed in the data around $L/E_\nu = 500$ km GeV^{-1} is consistent with the expectation of the first oscillation minimum by two-flavor neutrino oscillations.

4.3. Detecting Tau Neutrinos

If oscillations between ν_μ and ν_τ occur, it should be possible to observe charged-current ν_τ interactions generated by neutrino oscillations. A charged-current ν_τ interaction produces a τ lepton that is typically accompanied by several hadrons, most of which are pions. Due to the heavy τ lepton mass (1.78 GeV/c^2), the threshold for this interaction is ~3.5 GeV. The lifetime of a τ lepton is 2.9×10^{-13} s. Thus, the produced τ lepton decays, typically within 1 mm, into several hadrons plus a neutrino with a branching ratio of 64%. A typical ν_τ interaction has several hadrons in the final state. However, the typical high-energy neutral-current interactions also produce several hadrons in the final state. Therefore, a search for ν_τ events in a water Cherenkov detector may not be easy to perform due to these neutral-current background events. **Figure 11** shows a simulated charged-current ν_τ interaction in the Super-Kamiokande detector. Compared with **Figure 6**, the event pattern is complicated, with several overlapping images of Cherenkov rings in a single event.

The detection of ν_τ interactions poses another difficulty. Due to the high threshold for charged-current ν_τ interactions, together with the soft atmospheric neutrino flux, the expected event rate is only ~1 per kiloton per year, which corresponds to ~0.5% of the total atmospheric neutrino interactions.

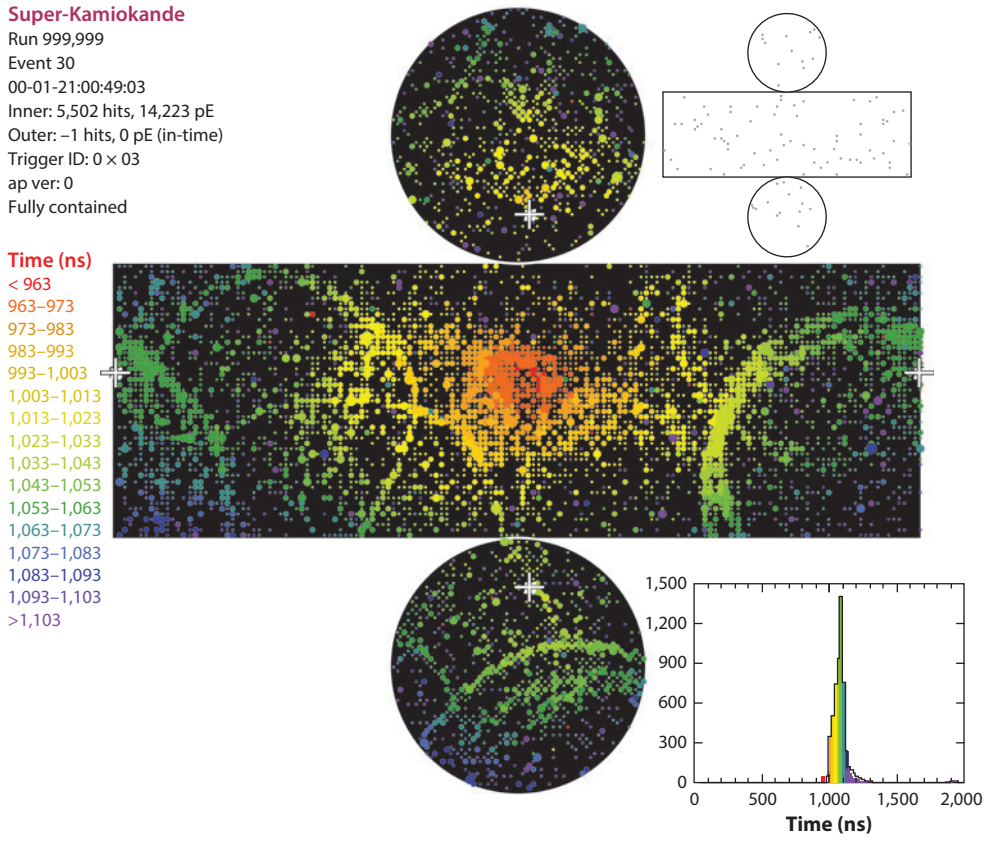

Figure 11

A simulated charged-current ν_τ interaction in the Super-Kamiokande detector.

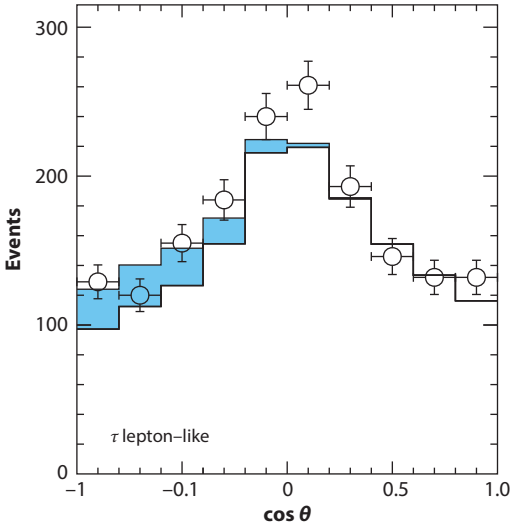

Figure 12

Zenith-angle (θ) distributions for the τ-like events selected from Super-Kamiokande data (47). The circles with error bars represent the data. The white histograms represent the Monte Carlo prediction with $\nu_\mu \rightarrow \nu_\tau$ oscillations but without the charged-current ν_τ interactions. The blue histograms represent the fit result with the ν_τ interactions included.

The Super-Kamiokande Collaboration (47) has searched for charged-current ν_τ interactions by using various kinematical variables with an advanced analysis method (i.e., the artificial neural-network method). **Figure 12** shows the zenith-angle distribution for candidate ν_τ events from Super-Kamiokande. Even with the selection of τ-like events, there are still many background events. However, note that there is an excess of upward-going events that cannot be explained by the background events. The best-fit number of ν_τ interactions that occurred in the fiducial volume of the detector during the 2,806-day exposure was $180.1 \pm 44.3(\text{stat.})^{+17.8}_{-15.2}(\text{syst.})$ (47). The expected number was $120.2^{+34.2}_{-34.8}$. One of the largest systematic errors in the previous analysis (48) was due to the unknown value of θ_{13}, that is, the unknown contribution of the electron appearance events in the upward-going τ-like sample. The accurately measured value of θ_{13} (38–42) has a significant role in reducing the systematic error in the ν_τ appearance. The significance of the excess, taking various systematic uncertainties into account, is 3.8σ. The data are indeed consistent with the ν_τ appearance due to $\nu_\mu \rightarrow \nu_\tau$ oscillations.

4.4. Three-Flavor Neutrino Oscillations

Recent data from the reactor neutrino oscillation experiments (Daya Bay, RENO, and Double Chooz), as well as those from long-baseline experiments (T2K and MINOS), showed that $\sin^2\theta_{13} = 0.024$ to 0.0255, depending on the mass hierarchy and on the global analysis (49–51). [Note, however, that depending on the data used in the global fit, a possibility remains that $\sin^2\theta_{13}$ is slightly smaller than the above range (51).] Although the atmospheric neutrino oscillations are dominated by $\nu_\mu \rightarrow \nu_\tau$ oscillations, three-flavor oscillation effects should be visible at some level. With the observation of nonzero θ_{13}, one wonders whether atmospheric neutrino experiments can determine the mass hierarchy or the *CP* phase (δ_{CP}) in the neutrino mixing matrix (Equation 3).

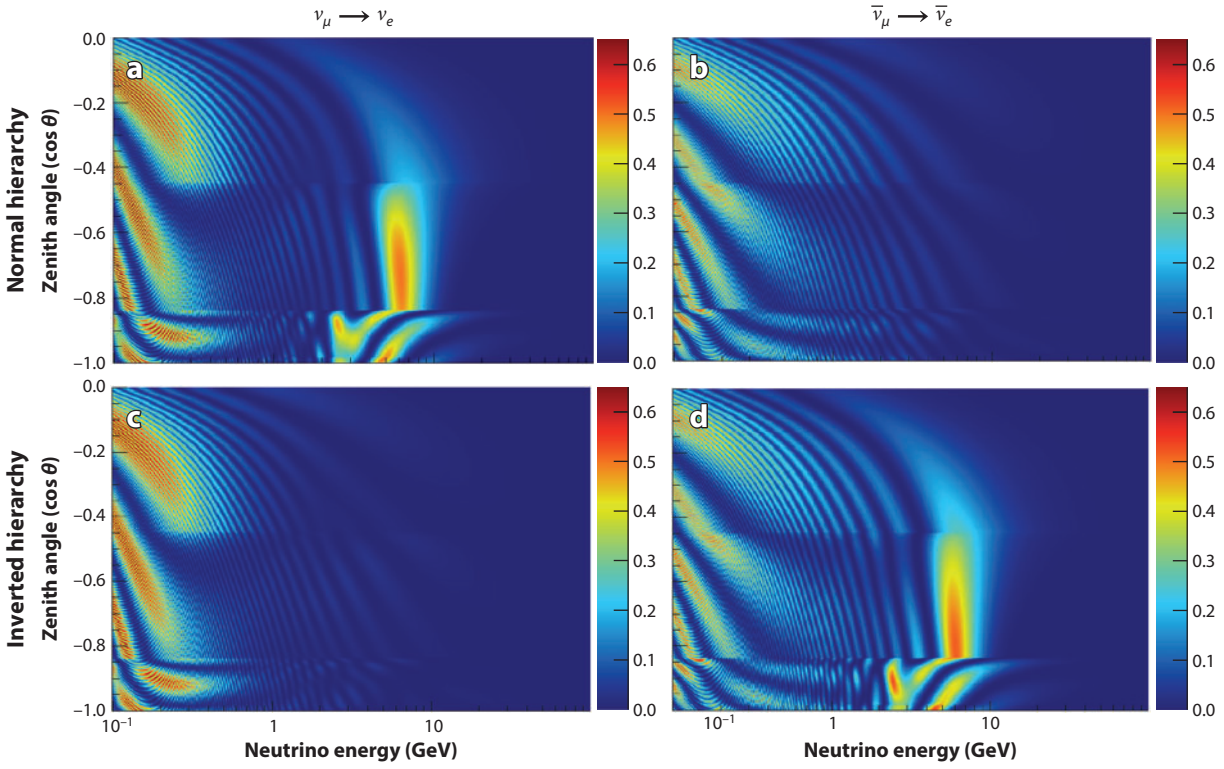

Figure 13

Oscillation probability $P(\nu_\mu \rightarrow \nu_e)$ as a function of the neutrino energy and zenith angle ($\cos\theta$) for (*a*,*c*) neutrinos and (*b*,*d*) antineutrinos and for the (*a*,*b*) normal and (*c*,*d*) inverted mass hierarchies. (*a*,*d*) The high-oscillation probabilities in the upward-going, multi-GeV region represent the matter resonance due to nonzero θ_{13}. The high-oscillation probabilities in the upward-going, sub-GeV region in all four panels represent the oscillations due to θ_{12} and $\Delta m_{12}{}^2$. The oscillations observed between the two energy regions show the interference effects.

Because the three-flavor oscillations include ν_es, we write the oscillation effects as follows:

$$\left(\frac{F^{\rm osc}_{\nu_e}}{F^{0}_{\nu_e}}\right) = \Delta_1(\theta_{13}) + \Delta_2(\Delta m^2_{12}, \theta_{12}) + \Delta_3(\theta_{13}, \Delta m^2_{12}, \theta_{12}, \delta_{CP}), \qquad 5.$$

where $F^{\rm osc}_{\nu_e}$ and $F^{0}_{\nu_e}$ are the atmospheric ν_e fluxes with and without oscillations, respectively, and Δ_i is the change in ν_e flux due to oscillations in matter driven by the parameters in parentheses. In Equation 5, the matter effect plays an important role. **Figure 13** shows the oscillation probability $P(\nu_\mu \rightarrow \nu_e)$ as a function of the neutrino energy and zenith angle ($\cos\theta$) for neutrinos and antineutrinos propagating in the Earth and for the normal and inverted mass hierarchies. Atmospheric neutrino experiments are sensitive to all the Δ_is in Equation 5 to some extent. Because the matter enhancement of oscillations is effective for neutrinos (antineutrinos) and not for antineutrinos (neutrinos) for the normal (inverted) mass hierarchy, and because neutrino and antineutrino interactions differ in several ways, it might be possible to determine the mass hierarchy with atmospheric neutrino data. The interference term (δ_{CP}) may also play an important role in atmospheric neutrino oscillations. In fact, some authors (e.g., Reference 52) had indicated that the full three-flavor oscillation analysis may be important in atmospheric neutrino experiments, even before the discovery of nonzero θ_{13}.

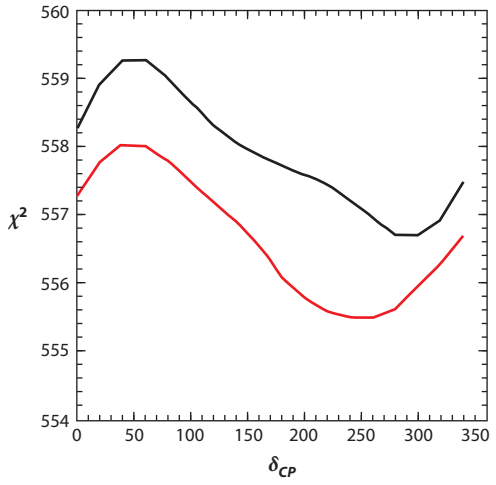

Figure 14

χ^2 distribution as a function of δ_{CP} for normal (*black line*) and inverted (*red line*) hierarchies from a full three-flavor neutrino oscillation analysis of Super-Kamiokande data.

The Super-Kamiokande Collaboration (43) has carried out a full three-flavor analysis. **Figure 14** shows the χ^2 distributions as a function of δ_{CP} for normal and inverted hierarchy assumptions. The χ^2 values differ somewhat, depending on the mass hierarchies and δ_{CP}: The χ^2 difference between the best-fit δ_{CP} point and the worst-fit point is ~2.5 for both normal and inverted mass hierarchies. The minimum χ^2 value for the inverted mass hierarchy is 1.2 lower than that of the normal mass hierarchy. Clearly, the present data cannot determine the mass hierarchy. However, this result suggests that future atmospheric neutrino experiments might be able to do so. Finally, we refer readers to the global analysis results (49–51).

5. FUTURE PROSPECTS

Present results from Super-Kamiokande suggest that future atmospheric neutrino experiments, with much higher event statistics or with a much better separation of neutrino and antineutrino events, should be able to determine the mass hierarchy and constrain the *CP* phase. Sensitivity studies with various detector technologies have been carried out.

Hyper-Kamiokande (53) will be a very large water Cherenkov detector with a fiducial mass of 0.56 megatons. Hyper-Kamiokande plans to determine the mass hierarchy by observing the matter resonance effect, as shown in **Figure 13**. Defining the sensitivity as the χ^2 difference between the normal and inverted mass hierarchies, and assuming that $\sin^2\theta_{23} = 0.5$ and $\sin^2\theta_{13} = 0.025$, one will be able to determine the mass hierarchy at a level better than 3σ within 5 to 10 years of operation (53).

The effects of the mass hierarchy, namely the matter effect due to θ_{13}, on the ν_μ flux are somewhat smaller. However, if the charge and the momentum of a muon are measured, then the detector will be sensitive to the mass hierarchy. **Figure 15** demonstrates the hierarchy sensitivity from $P(\nu_\mu \rightarrow \nu_\mu)$ (normal hierarchy) $- P(\nu_\mu \rightarrow \nu_\mu)$ (inverted hierarchy) for $\sin^2 2\theta_{13} = 0.1$ and for two different zenith angles (54). The India-Based Neutrino Observatory (INO) will utilize this quality. The iron calorimeter (ICAL) detector at INO will be a 50-kiloton detector with a 1.5-T magnetic field (55). With the present value of $\sin^2 2\theta_{13}$, ICAL will be able to determine the mass hierarchy, although it may take more than 10 years to reach the 3σ level (55).

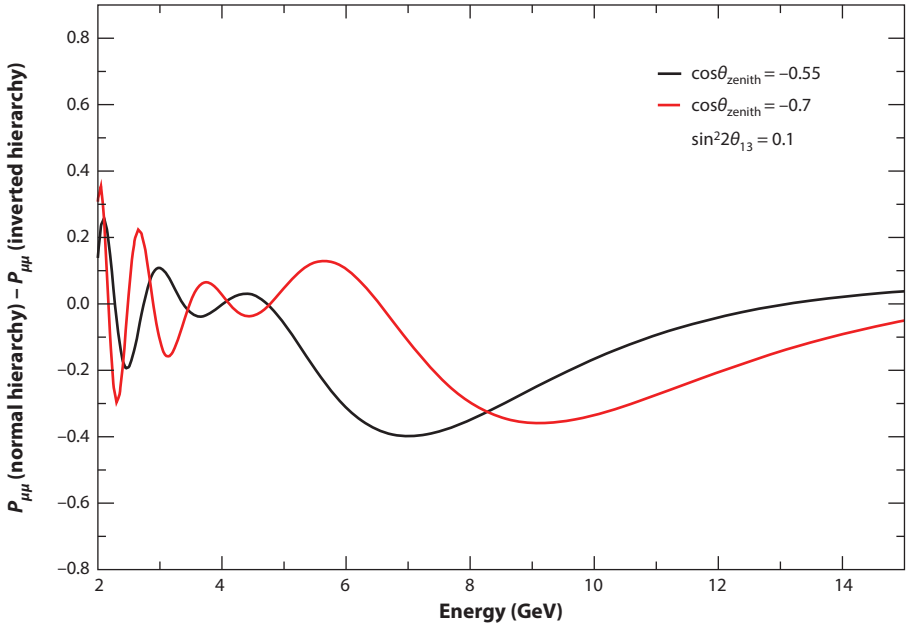

Figure 15

$P(\nu_\mu \to \nu_\mu)$ (normal hierarchy) − $P(\nu_\mu \to \nu_\mu)$ (inverted hierarchy) for $\sin^2 2\theta_{13} = 0.1$ and for $\cos\theta_{zenith} = -0.55$ (*black*) and −0.7 (*red*).

Another proposal is to install additional 20–40 strings (PINGU) in IceCube's existing DeepCore detector at the South Pole (56). As shown in **Figure 15**, the ν_μ survival probability depends on the mass hierarchy as a function of the zenith angle and the neutrino energy. Due to its huge fiducial mass (∼10 megatons) and a lower energy threshold than that of DeepCore, PINGU would be sensitive to the mass hierarchy. Depending on different analysis assumptions, it may be possible to determine the mass hierarchy with 3 years' worth of data at the 3.5–6σ level (56).

Finally, note that water Cherenkov detectors are sensitive to the octant of θ_{23} (θ_{23} larger or smaller than 45°) and δ_{CP} due to the possibility of observing subleading effects in the sub-GeV to GeV energy region. Even if $\sin^2 2\theta_{23} = 0.99$, it will be possible to determine the octant of θ_{23} at 90% CL for the present value of $\sin^2 2\theta_{13}$ (53). Future atmospheric neutrino experiments will have some sensitivity to δ_{CP} (53). However, it is also true that the sensitivity is limited compared with the planned accelerator-based long-baseline experiments. Atmospheric neutrino experiments will probably provide an independent confirmation of the accelerator results on *CP* violation. Some of the planned long-baseline experiments will not have long enough baselines to determine the mass hierarchy. If the mass hierarchy is not known, then δ_{CP} cannot be uniquely determined. The determination of the mass hierarchy with future atmospheric neutrino experiments may help eliminate the false *CP* solution in long-baseline experiments. In this sense, future atmospheric neutrino and long-baseline experiments will be complementary.

6. SUMMARY

This review describes studies of neutrino properties, namely oscillations, in atmospheric neutrino experiments. The L/E_ν range in atmospheric neutrinos is very wide. Therefore, atmospheric neutrinos represented a natural means of discovering neutrino oscillations when the neutrino

masses were unknown. Following early studies of atmospheric neutrinos, neutrino oscillation was discovered in 1998. In the following 15 years, both the data and our understanding of the neutrino oscillations substantially improved.

It is widely believed that the discovery of the neutrino masses opened a window to new physics beyond the Standard Model. In fact, the seesaw mechanism of neutrino mass suggests that small neutrino masses may indicate new physics at a very high mass scale. In fact, the observed Δm^2 values suggest that the physics involved in the masses of neutrinos may be related to the Grand Unification of elementary particles. In addition, the large mixing angles may aid our understanding of the relation between quarks and leptons. The small but finite neutrino masses may also be the key to understanding the baryon–antibaryon asymmetry in the Universe (57). Largely motivated by this physics, new proposals and ideas for future atmospheric neutrino experiments have been extensively discussed. Atmospheric neutrino experiments will probably continue to contribute to studies of neutrino properties.

DISCLOSURE STATEMENT

The author is not aware of any affiliations, memberships, funding, or financial holdings that might be perceived as affecting the objectivity of this review.

ACKNOWLEDGMENTS

The author thanks his colleagues at Super-Kamiokande. This work was partly supported by the Japanese Ministry of Education, Culture, Sports, Science, and Technology; a Grant-in-Aid in Scientific Research supported by the Japan Society for the Promotion of Science; and the European Union FP7-funded project ITN Invisibles (Marie Curie Actions, PITN-GA-2011-289442).

LITERATURE CITED

1. Minkowski P. *Phys. Lett. B* 67:421 (1977)
2. Yanagida T. In *Proceedings of the Workshop on the Unified Theory and Baryon Number in the Universe*, ed. O Sawada, A Sugamoto, p. 95. Tsukuba, Jpn.: KEK (1979)
3. Gell-Mann M, Ramond P, Slansky R. In *Supergravity*, ed. P van Nieuwenhuizen, DZ Freedman, p. 315. Amsterdam: North-Holland (1979)
4. Maki Z, Nakagawa M, Sakata S. *Prog. Theor. Phys.* 28:870 (1962)
5. Pontecorvo B. *Sov. Phys. J. Exp. Theor. Phys.* 26:984 (1968)
6. Honda M, Kajita T, Kasahara K, Midorikawa S. *Phys. Rev. D* 83:123001 (2011)
7. Honda M, et al. *Phys. Rev. D* 75:043006 (2007)
8. Barr GD, et al. *Phys. Rev. D* 70:023006 (2004)
9. Battistoni G, Ferrari A, Montaruli T, Sala PR. *Astropart. Phys.* 19:269 (2003)
10. Kajita T, Lipari P. *C. R. Phys.* 6:739 (2005)
11. Achar CV, et al. *Phys. Lett.* 18:196 (1965)
12. Reines F, et al. *Phys. Rev. Lett.* 15:429 (1965)
13. Pati JC, Salam A. *Phys. Rev. D* 8:1240 (1973)
14. Georgi H, Glashow SL. *Phys. Rev. Lett.* 32:438 (1974)
15. Hirata KS, et al. *Phys. Lett. B* 205:416 (1988)
16. Casper D, et al. *Phys. Rev. Lett.* 66:2561 (1991)
17. Allison WWM, et al. (Soudan-2 Collab.) *Phys. Lett. B* 391:491 (1997)
18. Hirata KS, et al. *Phys. Lett. B* 280:146 (1992)
19. Fukuda Y, et al. *Phys. Lett. B* 335:237 (1994)
20. Fukuda Y, et al. *Nucl. Instrum. Methods A* 501:418 (2003)

21. Fukuda Y, et al. (Super-Kamiokande Collab.) *Phys. Rev. Lett.* 81:1562 (1998)
22. Kajita T (Kamiokande Collab., Super-Kamiokande Collab.) *Nucl. Phys. Proc. Suppl.* 77:123 (1999)
23. Allison WWM, et al. (Soudan-2 Collab.) *Phys. Lett. B* 449:137 (1999)
24. Ambrosio M, et al. (MACRO Collab.) *Phys. Lett. B* 434:451 (1998)
25. Ambrosio M, et al. (MACRO Collab.) *Phys. Lett. B* 478:5 (2000)
26. Aharmim B, et al. (SNO Collab.) *Phys. Rev. D* 80:012001 (2009)
27. Adamson P, et al. (MINOS Collab.) *Phys. Rev. D* 73:072002 (2006)
28. Adamson P, et al. (MINOS Collab.) *Phys. Rev. D* 86:052007 (2012)
29. Abbasi R, et al. (IceCube Collab.) *Phys. Rev. D* 83:012001 (2011)
30. Adrian-Martinez S, et al. (ANTARES Collab.) *Eur. Phys. J. C* 73:2606 (2013)
31. Aartsen MG, et al. (IceCube Collab.) *Phys. Rev. Lett.* 110:151105 (2013)
32. Adrian-Martinez S, et al. (ANTARES Collab.) *Phys. Lett. B* 714:224 (2012)
33. Aartsen MG, et al. (IceCube Collab.) *Phys. Rev. Lett.* 111:081801 (2013)
34. Wendell R, et al. (Super-Kamiokande Collab.) *Phys. Rev. D* 81:092004 (2010)
35. Aharmim B, et al. (SNO Collab.) *Phys. Rev. C* 88:025501 (2013)
36. Abe K, et al. (Super-Kamiokande Collab.) *Phys. Rev. D* 83:052010 (2011)
37. Abe S, et al. (KamLAND Collab.) *Phys. Rev. Lett.* 100:221803 (2008)
38. Abe Y, et al. (Double Chooz Collab.) *Phys. Rev. D* 86:052008 (2012)
39. Ahn JK, et al. (RENO Collab.) *Phys. Rev. Lett.* 108:191802 (2012)
40. An FP, et al. (Daya Bay Collab.) *Phys. Rev. Lett.* 108:171803 (2012)
41. Abe K, et al. (T2K Collab.) *Phys. Rev. D* 88:032002 (2013)
42. Adamson P, et al. (MINOS Collab.) *Phys. Rev. Lett.* 110:171801 (2013)
43. Itow Y. *Nucl. Phys. B Proc. Suppl.* 235/236:79 (2013)
44. Abe K, et al. (T2K Collab.) *Phys. Rev. Lett.* 111:211803 (2013)
45. Adamson P, et al. (MINOS Collab.) *Phys. Rev. Lett.* 110:251801 (2013)
46. Ashie Y, et al. (Super-Kamiokande Collab.) *Phys. Rev. Lett.* 93:101801 (2004)
47. Abe K, et al. (Super-Kamiokande Collab.) *Phys. Rev. Lett.* 110:181802 (2013)
48. Abe K, et al. (Super-Kamiokande Collab.) *Phys. Rev. Lett.* 97:171801 (2006)
49. Fogli GL, et al. *Phys. Rev. D* 86:013012 (2012)
50. Forero DV, Tortola M, Valle JWF. *Phys. Rev. D* 86:073012 (2012)
51. Gonzalez-Garcia MC, Maltoni M, Salvado J, Schwetz T. *J. High Energy Phys.* 1212:123 (2012)
52. Fogli GL, Lisi E, Marrone A, Palazzo A. *Prog. Part. Nucl. Phys.* 57:742 (2006)
53. Abe K, et al. arXiv:1109.3262 [hep-ex] (2011)
54. Choubey S. Presented at Int. Conf. Neutrino Phys. Astrophys., 25th (Neutrino2012), Kyoto, Jpn. (2012); Choubey S. *Nucl. Phys. B Proc. Suppl.* 235/236:87 (2013)
55. Athar MS, et al. (INO Collab.) *India-Based Neutrino Observatory: Project Report*. INO/2006/01. Mumbai: INO Collab. **http://www.ino.tifr.res.in/ino/OpenReports/INOReport.pdf** (2006)
56. Aartsen MG, et al. arXiv:1306.5846 [astro-ph] (2013)
57. Fukugita M, Yanagida T. *Phys. Lett. B* 174:45 (1986)